Modeling Connectivity and Asymmetry in Membrane Filters

Binan Gu[1], Dylan Renaud[2], Pejman Sanaei[3], Lou Kondic[1], Linda J. Cummings[1]

[1]Department of Mathematical Sciences, New Jersey Institute of Technology, Newark, NJ 07102-1982, USA
[2]Department of Physics, Harvard University, Cambridge, MA 02138
[3]Courant Institute of Mathematical Sciences, New York University, New York, NY 10012-1110, USA

Emails: [1]bg263@njit.edu

1. Introduction

Membrane filters have a wide range of industrial and commercial applications. Water purification, beer clarification and radioactive sludge removal, among many other processes, have all benefited from the use of filters capable of microfiltration or ultrafiltration. There is considerable industrial interest in designing and manufacturing layered filters that allow for fine control of particle removal while maintaining a reasonable filter lifetime. Such filters typically have pore size that decreases from one layer to the next (in the direction of flow, see Figure 1(a)). In this way, more uniform fouling throughout the filter is achieved, since fouling begins at the upstream side of the membrane, and thus the fouling rate is a decreasing function of depth through the membrane (as is the concentration of particles in the feed). Such layered structures may incorporate varying degrees of *connectivity* between pores in different layers, seen in Figure 1(b). In addition to connectivity considerations, another inevitable geometric feature of industrial filters is that the pore sizes within each layer vary due to imperfect manufacturing (see figure 1(c)), which we refer to as *asymmetry* in all subsequent discussions.

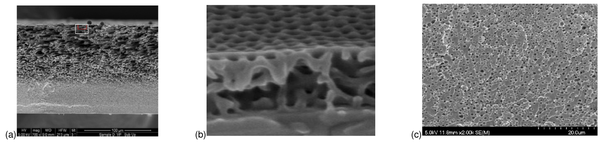

Figure 1: *Membrane images showing (a) gradation of pores sizes through membrane depth, and in-plane inhomogeneity of pore sizes; (b) connectivity and (c) various pore size distributions.*

Membrane fouling occurs by three principal mechanisms: 1) *adsorption*, an accretion process in which small particles adhere to the pore walls and thus shrink the effective radius of the pore; 2) *blocking*, a discrete process in which particles larger than pores cover partially or completely the entrance of a pore; 3) *caking*, in which an additional layer of porous medium, composed of the particles carried by the flow, forms on top of the membrane surface, occurring particularly in the later stages of a membrane filtration process. Here we consider adsorption as the dominant fouling mechanism.

2. Mathematical Model

Governing Equations

We consider layered membranes in which pores within a given layer are modeled as circular cylinders spanning the layer. Two suffices are used to denote pore locations within the membrane, the first denoting the layer (numbered from the upstream surface, with a total of m layers), and the second denoting position within the layer (ν_i pores in layer i). Flow is driven by a uniform pressure drop P_0 across the membrane. Incompressibility (mass conservation) conditions for the fluid yield

$$\text{(local flux)} \quad \frac{\partial Q_{ij}}{\partial X} = 0, \quad Q_{ij} = \pi A_{ij}^2 \overline{U}_{\mathrm{p},ij}, \quad 1 \le i \le m, \quad 1 \le j \le \nu_i, \tag{1}$$

Q_{ij} : local flux, $\overline{U}_{\mathrm{p},ij}$: local pore velocity, A_{ij} : pore radius, ν_i : number of pores in the i-th layer. (2)

Flux conservation (figure 2) allows for non-uniform splitting of the flow at each junction. The inter-layer junction regions are assumed to have negligible resistance (uniform pressure regions). Global superficial Darcy velocity U and flux Q are then given by

$$\text{(global flux)} \quad Q = (2W)^2 U = \sum_{j=1}^{\nu_i} \pi A_{ij}^2 \overline{U}_{\mathrm{p},ij}, \quad 1 \le i \le m. \tag{3}$$

The junction regions are assumed to be sufficiently low-resistance that pressure is spatially uniform within them. A Hagen-Poiseuille model for pore j within layer i then gives

$$\text{(Hagen-Poiseuille)} \quad Q_{ij} = -\frac{1}{\mu R_{ij}} \frac{P_i - P_{i-1}}{D_i}, \quad R_{ij} = \frac{8}{\pi A_{ij}^4}, \quad 1 \le i \le m, \quad 1 \le j \le \nu_i. \tag{4}$$

Continuity of flux, $Q = \sum_{j=1}^{\nu_i} Q_{ij}$ leads to

$$\text{(total resistance)} \quad Q = (2W)^2 U = \frac{P_0}{\mu R}, \quad R = \sum_{i=1}^{m} D_i \left(\sum_{j=1}^{\nu_i} \frac{1}{R_{ij}} \right)^{-1}, \tag{5}$$

where R is the total resistance of the membrane.

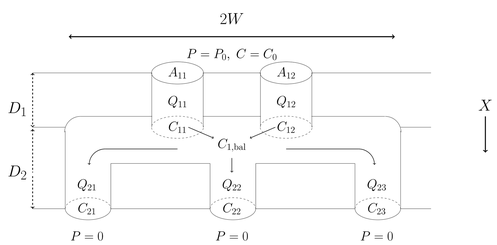

Figure 2: *Schematic of a connected branching pore membrane. Flow is in the X-direction. The structure here consists of $m = 2$ layerswith pressure drop P_0 and upstream particle concentration C_0.*

Foulants Transport and Deposition

Asymptotic analysis of the advection-diffusion equation governing particle transport down pores reveals that diffusion dominates radially, leading to particle concentration that is approximately uniform across the pore cross-section, while concentration varies in the X-direction according to

$$\overline{U}_{\mathrm{p},ij} \frac{\partial C_{ij}}{\partial X} = -\Lambda \frac{C_{ij}}{A_{ij}}, \quad X_{i-1} \le X \le X_i, \quad 1 \le i \le m, \quad 1 \le j \le \nu_i, \tag{6}$$

where C_{ij} is the cross-sectionally averaged particle concentration in the pore i, j and Λ a dimensional deposition coefficient. The upstream condition is $C_{01}(T) = C_0$, and particle concentration is continuous at layer junctions. We assume further that uniform particle mixing occurs in the junctions, so that particle concentration is a function only of T in junctions, with $C_{i,\mathrm{bal}}$, the concentration in the junction below layer i given by

$$C_{i,\mathrm{bal}} := \frac{\sum_{j=1}^{\nu_i} Q_{ij} C_{ij}}{\sum_{j=1}^{\nu_i} Q_{ij}}, \quad 1 \le i \le m, \tag{7}$$

Spatial Discretization

To save computational time in the large number of simulations we wish to carry out, we use a coarse-grained finite difference approximation, $\frac{\partial C_{ij}}{\partial X} \approx \frac{C_{ij} - C_{i-1,\mathrm{bal}}}{D_i}$ (simulations were checked for accuracy). The concentrations within each pore then satisfy

$$C_{ij} = \frac{\overline{U}_{\mathrm{p},ij} C_{i-1,\mathrm{bal}}}{\overline{U}_{\mathrm{p},ij} + \Lambda D_i / A_{ij}}, \quad C_{0,\mathrm{bal}} = C_0, \quad 1 \le i \le m, \quad 1 \le j \le \nu_i, \tag{8}$$

and the radius of pore j in the i-th layer evolves at the following rate

$$\frac{\partial A_{ij}}{\partial T} = -\Lambda \alpha C_{i-1,\mathrm{bal}}, \quad 1 \le i \le m, \quad 1 \le j \le \nu_i. \tag{9}$$

3. Results

We present our results in non-dimensional form by introducing variables and parameters:

$$P_{ij} = P_0 p_{ij}, \quad (X, D_i) = D\,(x, d_i), \quad C_{ij} = C_0 c_{ij}, \quad A_{ij} = W a_{ij}, \quad \left(U, \overline{U}_{\mathrm{p,ij}}\right) = \frac{\pi W^2 P_0}{32 \mu D \hat{r}_0} \left(u, \overline{u}_{\mathrm{p,ij}}\right), \quad T = \frac{W}{\Lambda \alpha C_0} t,$$

$$r = \frac{1}{\hat{r}_0} \sum_{i=1}^{m} d_i \left(\sum_{j=1}^{\nu_i} a_{ij}^4 \right)^{-1}, \quad V = \frac{(2W)^2 D}{\alpha C_0} v, \qquad v\,(t) = \frac{1}{\lambda} \int_0^t u\left(0, t'\right) dt',$$

where V and v are the dimensional and dimensionless total throughput (i.e. total volume of filtrate collected at membrane outlet); λ is the dimensionless deposition coefficient. We make comparisons of membranes of equal initial resistance, assuming that pore size varies geometrically from one layer to the next with geometric parameter κ. With all pore in a given layer identical, pore structure is determined by three parameters: $a_1(0)$, κ and ϕ_{top} (porosity of top layer). We have

$$a_i(0) = a_1\,(0)\,\kappa^{i-1}, \quad \phi_{\mathrm{top}} = \nu_1 \pi a_1\,(0)^2 / 4, \tag{10}$$

For fixed resistance only two can be specified.

Symmetric Models

Figure 3 depicts flux versus throughput results for two- and single-inlet connected and single-inlet non-connected membranes of equal resistance but variable top layer porosity. The best throughput performance is realized when ϕ_{top} is maximized. We note that both single-inlet models show strikingly similar performance: lower-layer morphology and connectivity play only a minor role here.

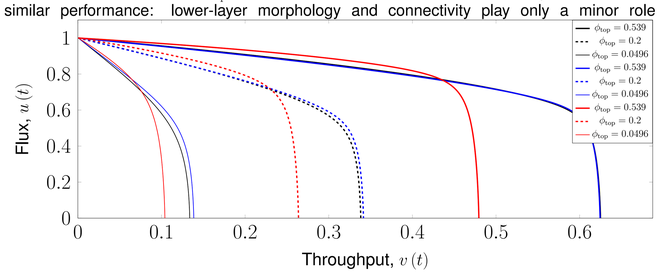

Figure 3: *Symmetric Models: Flux versus throughput for non-connected (black), single-inlet connected (blue), and two-inlet connected (red) membrane structures.*

Figure 4(a) shows how particle concentration varies in time t for connected membrane structures (single- and two-inlet). Figure 4(a) shows the concentration in the filtrate, as a function of throughput. Note that for large pore-size gradients (small κ) particle concentration in the filtrate may actually increase during the filtration. This behavior could be due to high pore velocity in this situation, see figure 4(b), advecting particles rapidly through the membrane before they can adhere.

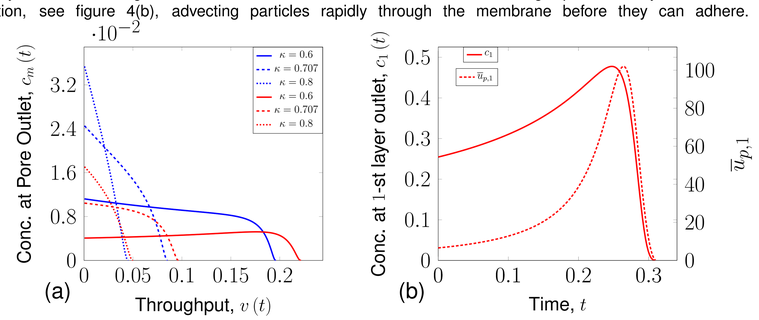

Figure 4: *Symmetric Models: (a) Concentration at pore outlet vs. throughput for single-inlet connected (blue) and two-inlet connected (red) membrane structures. (b) Concentration at first layer outlet (c_1, solid red curve) and cross-sectionally averaged first layer pore velocity ($\overline{u}_{p,1}$, dashed red curve) are shown.*

Asymmetric Models

To investigate in-plane asymmetry, the same layered structure is considered, but pores are no longer identical within layers. For each model, pore radii are changed individually by introducing a random perturbation onto the symmetric pore radii. More precisely, the initial radius of the j-th pore in the i-th layer is now given by

$$\tilde{a}_{ij}(0) = a_i(0)(1 + \epsilon_{ij}), \quad \epsilon_{ij} \sim \mathrm{unif}(-b, b), \quad 0 \le b \le 1, \tag{11}$$

where $a_i(0) = a_1\,(0)\,\kappa^{i-1}$ as in the symmetric case and ϵ_{ij} is a uniform random variable on $[-b, b]$. Figure 5 shows how results depend on the perturbation amplitude b. We observe that the greater the noise amplitude, the larger the total throughput. In general, both connected models exhibit monotonically increasing total throughput as b increases. However, closer attention reveals that for certain choices of the geometric coefficient κ, the average initial flux $\overline{u}_b(0)$ actually decreases when b increases but is kept small. This is illustrated in figure 5(a), where $\kappa = 0.95$. Here we find that $\overline{u}_b(0)$ decreases for small values of b before recovering after a critical value of b.

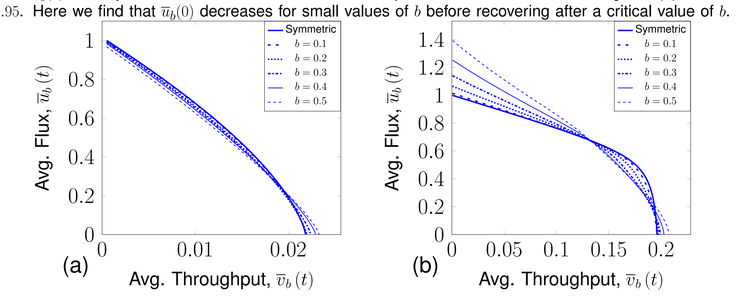

Figure 5: *Asymmetric Models: Average flux versus throughput for single-inlet connected models for varying noise amplitude, b. (a) $\kappa = 0.95$, and (b) $\kappa = 0.6$. Results are averaged over 10^4 simulations.*

It is not immediately clear why average initial flux should decrease as perturbations become more noisy (with our chosen parameters). We are, however, able to find an explicit formula for the expected initial resistance, which provides mathematical foundation for this phenomenon:

$$\mathbb{E}\left[r_b(0)\right] = \frac{a_0^{-4}}{\hat{r}_0} \sum_{i=1}^{m} d_i \kappa^{-4(i-1)} \int_0^{\infty} \left[\frac{1}{8bs^{\frac{1}{4}}} \left[\gamma\left(\frac{1}{4}, s\,(1+b)^4\right) - \gamma\left(\frac{1}{4}, s\,(1-b)^4\right) \right] \right]^{\nu_i} ds, \tag{12}$$

where γ is the lower incomplete Gamma function. In figure 6, we showcase how sensitive the expected initial resistance is to changes in noise amplitude b. For selected κ values, $\mathbb{E}\left[r_b(0)\right]$ decreases for a range of small values in b and then eventually resumes its monotone increasing nature, in both proposed models.

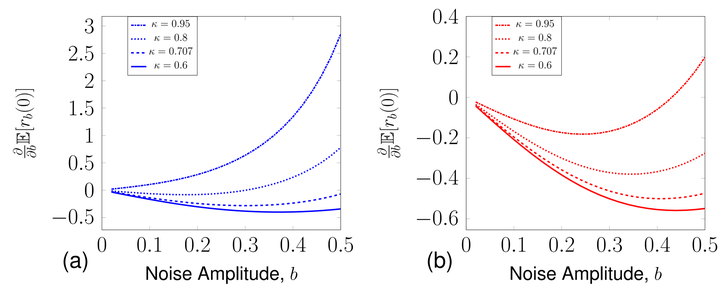

Figure 6: *Asymmetric Models: Partial derivative of expected initial resistance against noise amplitude versus noise amplitude, b, for the (a) single-inlet connected model and (b) two-inlet connected model.*

4. Conclusions

- The influence of connectivity is more pronounced in asymmetric membranes via concentration rebalance in junction regions.
- The relative performance of non-connected and connected membranes does not strongly depend on either intra-layer connections or surface porosity.
- Larger top layer porosity leads to longer membrane lifetimes.
- For certain morphology parameter choices, the concentration of particles leaving the membrane can increase over time.
- In the asymmetric regime, one can no longer claim a Darcy-type relation $u = 1/r$ for the averaged flux and resistance.

5. Acknowledgements

The authors acknowledge financial support from the NSF under grant DMS-1615719.